The 1st Joint International Conference on Multibody System Dynamics
May 25–27, 2010, Lappeenranta, Finland

Efficient and Accurate Simulation of the Cable–Pulley Interaction in Weight–Lifting Machines

Urbano Lugrís*, José L. Escalona#, Daniel Dopico*, Javier Cuadrado*

* Escuela Politécnica Superior
University of La Coruña
Mendizábal s/n, 15403 Ferrol, Spain
e-mail: ulugris@udc.es

Escuela Superior de Ingenieros
University of Sevilla
Camino de los Descubrimientos s/n, 41092 Sevilla, Spain
e-mail: escalona@us.es

ABSTRACT

This paper presents different approaches that can be used for modeling cables in weight–lifting machines. It is shown that modeling the cable as a linear spring, although very simple and efficient, is energetically inconsistent and produces spurious terms in the equations of motion if the cable deformation along the segment in contact with the pulley is not considered. In order to overcome this problem and obtain an efficient yet accurate method for the simulation of such systems, a semi–analytical method is derived by introducing an analytical model of the cable–pulley interaction [10] in the system, and the obtained results are compared to a finite–element numerical model. The semi–analytical model is based on a continuum mechanics approach of the cable; it assumes Coulomb friction between the pulley and the cable and neglects the inertia of the segment of cable in contact with the pulley. The numerical model is based on the Absolute Nodal Coordinate Formulation (ANCF) [13], and accounts for both the inertia forces and the bending and axial deformation of the cables.

Keywords: Cable–pulley interaction, contact, friction, flexible multibody dynamics, ANCF.

1 INTRODUCTION

The literature about cable–pulley interaction in weight lifting machines is not very frequent, at least from the multibody dynamics point of view. However, the interaction between belts and pulleys in belt–drives, which is a very similar problem, has been studied by several authors in the past, such as Leamy and Wasfy [12], Kerkkanen et al. [11] or Čepon and Boltežar [14].

In the present work, two different approaches for simulating weight lifting machines based on cable–pulley systems are introduced and compared. The first one is an efficient semi–analytical model, which accounts for the cable–pulley friction forces and the axial deformation of the segment of cable in contact with the pulley. The second one uses the Absolute Nodal Coordinate Formulation [13] as done by Kerkkanen et al., although it uses a different approach for obtaining the elastic forces [1], and a contact model that is better suited for the operation conditions of weight lifting machines [3, 8].

2 MODELING CABLES AS LINEAR SPRINGS

Modeling cables as linear springs is very simple and efficient approach that is reasonable in many practical applications. However when the machine includes cable–pulley mechanisms this approach may be energetically inconsistent and spurious forces may appear in the equations of motion. A simple model is used next to show these facts. Figure 1(a) shows the simple model of an elevator that will be used throughout this paper. The elevator model consists of a pulley driven by an electrical motor, the cabin and the counterweight that are connected to the pulley through a cable. Three coordinates are selected to describe the dynamics of the elevator namely the pulley angle θ, the elongation of the segment of the cable at the cabin side y_{cab} and the elongation of the segment of the cable at the counterweight side y_{cw}. Assuming that the cable segments behave as linear springs with variable stiffness, the equations of motion for the elevator yield:

$$\mathbf{M}\ddot{\mathbf{q}} + \mathbf{K}(\theta) = \mathbf{Q}^{grav} + \mathbf{Q}_{nl}^{elas} + \mathbf{Q}^{driv} \tag{1}$$

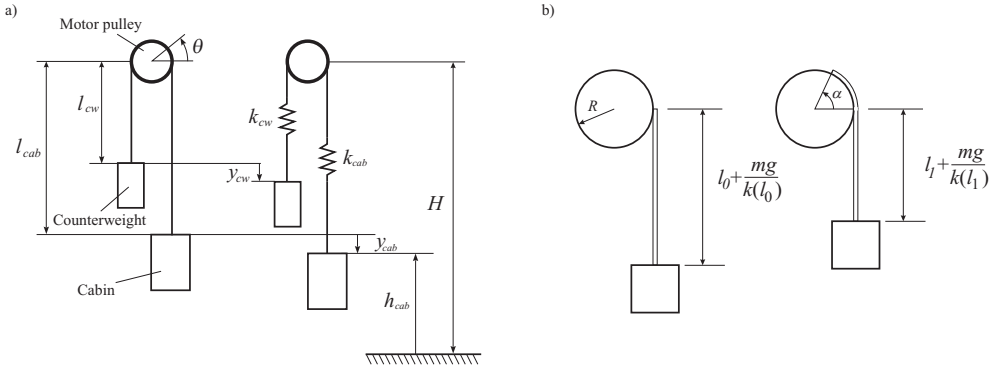

Figure 1. a) simple elevator model. b) quasi–stacic weight lifting

where $\mathbf{M}$ is a constant mass matrix and $\mathbf{K}$ is a stiffness matrix that depends on the angle θ rotated by the pulley due to the change in length of the cable segments. The non–linear elastic force vector $\mathbf{Q}_{nl}^{elas}$ is the partial derivative of the deformation energy with respect to θ. $\mathbf{Q}_{nl}^{elas}$ contains forces with no physical meaning. Generalized force vectors $\mathbf{Q}^{grav}$ and $\mathbf{Q}^{driv}$ are due to gravity forces and the motor torque, respectively.

The energy balance of the pulley–cable system when quasi–statically lifting a weight shows that the previously defined cable model is energetically inconsistent. Figure 1(b) shows the initial and final instants. In both positions the cable is assumed to be in static equilibrium. Assuming the center of the pulley as the level of zero gravitational energy, the potential energy of the system at the initial and final positions, 0 and 1, is given by:

$$U_i = -mg\left(l_i + \frac{mg}{k(l_i)}\right) + \frac{1}{2}k(l_i)\left(\frac{mg}{k(l_i)}\right)^2, \quad i = 0, 1 \tag{2}$$

where $k(l_i) = EA/l_i$ is the cable instantaneous stiffness. Assuming that the pulley rotates an angle α such that $l_1 - l_o = \alpha R$, the increase in potential energy of the system is given by:

$$U_1 - U_0 = mg\left(1 + \frac{mg}{2EA}\right)\alpha R \tag{3}$$

The work delivered by the motor that drives the system from position 0 to position 1 is calculated as the product of the moment due to the weight times the angle rotated by the pulley, as follows:

$$W = mgR\alpha \tag{4}$$

Clearly the principle of work and energy is not fulfilled in this example since:

$$W \neq U_1 - U_0; \quad (U_1 - U_0) - W = \frac{(mg)^2}{2EA}\alpha R \tag{5}$$

Therefore some energy is artificially introduced into the system if the deformation energy of the cable segment in contact with the pulley is not considered. A model that accounts for the deformation of the length of the cable in contact with the pulley is necessary for an energetically consistent cable–pulley model.

3 DEFORMATION MODEL OF THE CABLE

This section describes a deformation model for the cable that accounts for the cable segment in contact with the pulley. The model is based on the theory of steady motion of belts and pulleys [10]. Figure 2 shows the cable–pulley contact segment, the normal contact stress distribution $p(\alpha)$ and the tangential contact stress distribution $t(\alpha)$. Assuming that the contact angle α varies form 0 to 180º and the tensile force T_2 is larger than T_1, the tangential contact stress distributions and the tensile force distribution are given by:

$$T(\alpha) = \begin{cases} T_1 e^{\mu\alpha} & \alpha \in [0, \beta] \\ T_2 & \alpha \in [\beta, \pi] \end{cases} \qquad t(\alpha) = \begin{cases} \dfrac{\mu T_1}{R} e^{\mu\alpha} & \alpha \in [0, \beta] \\ 0 & \alpha \in [\beta, \pi] \end{cases} \tag{6}$$

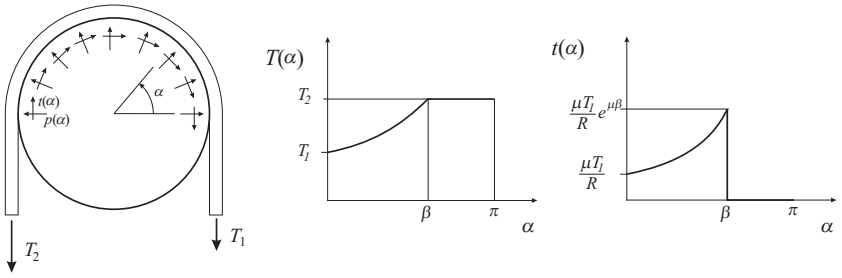

Figure 2. Contact force distribution at cable–pulley interaction.

where $\alpha \in [0, \beta]$ is the cable–pulley slip arc and $\alpha \in [\beta, \pi]$ is the cable–pulley stick arc. The transition angle is given by $\beta = 1/\mu \log(T_1/T_2)$, where μ is the friction coefficient. Unless the tensile forces at both branches of the cable have the same value, there is always a slip arc in the cable–pulley contact. It is in that slip arc where the traction torque is transmitted from the pulley to the cables through the tangential contact stresses. Note that the tangential stresses vanish in the stick arc.

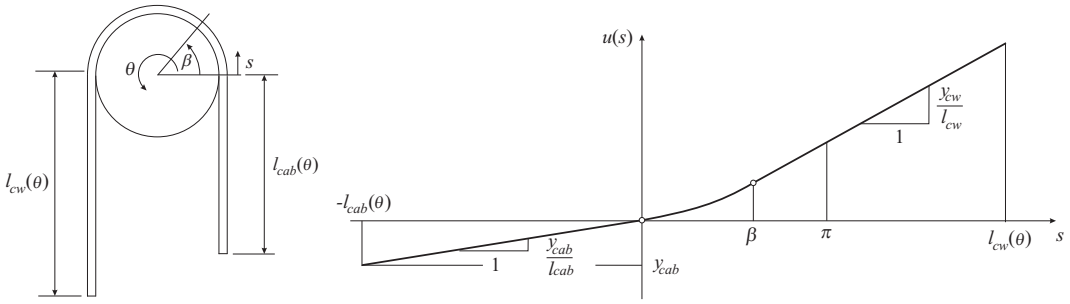

Figure 3. Cable axial displacement distribution.

In the deformation model it is assumed that the axial displacement due to deformation of any section of the cable can be obtained as a function of the generalized coordinates θ, y_{cab} and y_{cw} and the arc length parameter s (Figure 3) using a piecewise function. In case the tensile force at the cabin segment is larger than the tensile force at the counterweight segment, the function is given by:

$$u(s) = \begin{cases} s & -l_{cab} < s \leq 0 \\ \dfrac{y_{cab}}{l_{cab}} \left(e^{\mu s/R} - 1 \right) \dfrac{R}{\mu} & 0 < s \leq \beta R \\ \dfrac{y_{cw}}{l_{cw}} s + \left(\dfrac{y_{cw}}{l_{cw}} (1 - \mu\beta) - \dfrac{y_{cab}}{l_{cab}} \right) \dfrac{R}{\mu} & \beta R < s \leq \pi R + l_{cw} \end{cases} \tag{7}$$

This function has been selected such that it respects the tensile force distribution predicted by the theoretical results. As it can be seen in Figure 3, deformation, and therefore tensile force, is constant at the segments of the cable not in contact with the pulley. The tensile force grows exponentially in the slip angle of the pulley. Substituting the corresponding values at Eq. (7) it can be observed that the elongation of the cable attached to the cabin (low tension segment) is y_{cab}, however, the elongation of the cable attached to the counterweight (high tension segment) is no longer equal to y_{cw}. Therefore, the generalized coordinates have lost their original meaning.

The selected arc length parameter s has the origin at the entrance of the pulley in the side of the low tension cable segment. Therefore, the arc length parameter associated with a particular section of the cable is not constant but varies with time (with θ). Due to this reason, the velocity of the contact sections of the cable due to deformation is given by:

$$\dot{u} = \frac{\partial u}{\partial \mathbf{q}} \dot{\mathbf{q}} + \frac{\partial u}{\partial s} \dot{s} = \mathbf{u_q} \dot{\mathbf{q}} + u' R \dot{\theta} \tag{8}$$

where $u' = \partial u/\partial s$ is the cable axial deformation and $\dot{s} = R\dot{\theta}$ is the rate of change of the parameter s for any cable section. Since any cable section has a superimposed "rigid body velocity" $R\dot{\theta}$, the kinetic energy of the cable yields:

$$T_c = \frac{1}{2}\rho A_c \int_{-l_{cab}}^{\pi R + l_{cw}} \left[\mathbf{u_q}\dot{\mathbf{q}} + R\dot{\theta}(1+u')\right]^2 \, \mathrm{d}s \tag{9}$$

where ρA_c is the linear density of the cable. The deformation energy of the cable and gravitational potential energy are given by:

$$U_c^{def} = \frac{1}{2} E A_c \int_{-l_{cab}}^{\pi R + l_{cw}} (u')^2 \, \mathrm{d}s \tag{10}$$

$$U_c^{grav} = \rho A_c g \left[\int_{-l_{cab}}^{0} (s+u) \, \mathrm{d}s + \int_{0}^{\pi R} \left(u\cos\frac{s}{R} + R\sin\frac{s}{R} \right) \mathrm{d}s - \int_{\pi R}^{\pi R + l_{cw}} (s+u) \, \mathrm{d}s \right] \tag{11}$$

The kinetic and gravitational energies of the cabin, counterweight and motor–pulley (ccm) are given by:

$$T_{ccm} = \frac{1}{2} m_{cab} \, \dot{u}^2\big|_{s=-l_{cab}} + \frac{1}{2} m_{cw} \, \dot{u}^2\big|_{s=\pi R + l_{cw}} + \frac{1}{2} I_m \dot{\theta}^2 \tag{12}$$

$$U_{ccm}^{grav} = m_{cab} g \, (u - l_{cab})|_{s=-l_{cab}} - m_{cw} g \, (u + l_{cw})|_{s=\pi R + l_{cw}} \tag{13}$$

where the positions and velocities of the cabin and counterweight use the deformation field u particularized at the corresponding values of s. Finally, the virtual work of the tangential friction stresses between the cable and the pulley at the slip arc is given by:

$$\delta W^{fric} = -\int_0^{\beta R} t\,(s)\, \delta u \, \mathrm{d}s \tag{14}$$

where $\delta u = \mathbf{u_q}\delta\mathbf{q} + u' R \delta\theta$ is the virtual relative displacement between the cable sections and the pulley. According to Eq. (7), the tangential contact stress can be obtained as follows:

$$t\,(s) = \frac{1}{R}\frac{\mathrm{d}T(s)}{\mathrm{d}\alpha} = \frac{\mathrm{d}T(s)}{\mathrm{d}s} = E A_c u'' \tag{15}$$

where $u'' = \partial^2 u/\partial s^2$. Substituting Eq. (15) and the expression for δu in Eq. (14) yields:

$$\delta W^{fric} = -E A_c \int_o^{\beta R} u'' \left(\mathbf{u_q}\delta\mathbf{q} + u' R \delta\theta\right) \mathrm{d}s = \left(\mathbf{Q}^{fric}\right)^{\mathsf{T}} \delta\mathbf{q} \tag{16}$$

where $\mathbf{Q}^{fric}$ is the vector of generalized friction forces at the slip arc. This vector can be identified at Eq. (16) as:

$$\mathbf{Q}^{fric} = -\int_0^{\beta R} E A_c u'' \mathbf{u_q}^{\mathsf{T}} \, \mathrm{d}s + \int_0^{\beta R} E A_c u'' \begin{bmatrix} Ru' \\ 0 \\ 0 \end{bmatrix} \mathrm{d}s \tag{17}$$

Using the total kinetic energy of the system $T = T_{ccm} + T_c$ and the total potential energy of the system $U = U_{ccm}^{grav} + U_c^{grav} + U_c^{def}$ in Lagrange equations, the following equations of motion are obtained for the elevator model:

$$\mathbf{M}\ddot{\mathbf{q}} = \mathbf{Q}^{elas} + \mathbf{Q}^{grav} + \mathbf{Q}^{fric} + \mathbf{Q}^{driv} \tag{18}$$

where $\mathbf{Q}^{elas}$ + $\mathbf{Q}^{grav}$ are the non–linear elastic and gravity forces that result from the partial derivatives of U with respect to the system coordinates, and $\mathbf{Q}^{driv} = \begin{bmatrix} M^{driv}(t) & 0 & 0 \end{bmatrix}^{\mathsf{T}}$ is the generalized driving force being $M^{driv}(t)$ the driving torque applied by the motor.

The model previously explained is only valid when the cabin cable is the low tension segment. In case the counterweight segment becomes the low tension cable, the model and the system equations have to be changed by the alternative ones that are obtained accordingly.

4 DESCRIPTION OF THE ANCF BEAM ELEMENT

The absolute nodal coordinate formulation (ANCF) is a finite–element formulation specially designed for multibody system dynamics [13]. This is because the ANCF uses absolute positions and global slopes as nodal coordinates, thus eliminating the interpolation of finite rotations. The shape functions contain a full set of rigid–body deformation modes, so that finite elements can undergo large displacements and rotations without introducing spurious forces.

The total number of finite elements used for the cable discretization depends on the number of elements that are necessary for modeling the contact with the pulley. Using a large number of elements for the contact arc would allow for using a linear elastic forces formulation, but since the same element size must be kept along the total length of the cable, it would lead to a very large number of variables.

In order to overcome this problem, a nonlinear formulation based on continuum mechanics is used for modeling the elastic forces, more specifically a large–deformation planar beam element described by Berzeri and Shabana [1]. In this formulation, the effects of rotary inertia and shear strain are ignored, thus assuming the cross–sections to remain plane and perpendicular to the neutral axis. However, as opposed to other ANCF elements that use a floating reference frame to model the elastic forces [4], this formulation accounts for the nonlinearities due to large deformations, so that a smaller number of elements can be used for the discretization.

4.1 Kinematics

The position of an arbitrary point at the neutral axis of a finite element, $\mathbf{r}$, can be calculated by means of an interpolation matrix, $\mathbf{S}$, which, for a given element length l, depends on the material coordinate along the neutral axis in the undeformed configuration, x,

$$\mathbf{r}(\mathbf{e}, x) = \mathbf{S}(x)\mathbf{e} \tag{19}$$

The vector $\mathbf{e}$ is the vector of nodal variables, and it contains the absolute positions of the end nodes, along with their derivatives with respect to the material coordinate x, also known as *global slopes*,

$$\begin{Bmatrix} e_1 \\ e_2 \end{Bmatrix} = \mathbf{r}|_{x=0}\,, \quad \begin{Bmatrix} e_3 \\ e_4 \end{Bmatrix} = \left.\frac{\partial \mathbf{r}}{\partial x}\right|_{x=0}, \quad \begin{Bmatrix} e_5 \\ e_6 \end{Bmatrix} = \mathbf{r}|_{x=l}\,, \quad \begin{Bmatrix} e_7 \\ e_8 \end{Bmatrix} = \left.\frac{\partial \mathbf{r}}{\partial x}\right|_{x=l} \tag{20}$$

The matrix $\mathbf{S}$ is formed by a set of interpolation functions, s_i, arranged according to the following strutcure,

$$\mathbf{S} = \begin{bmatrix} s_1 & 0 & s_2 l & 0 & s_3 & 0 & s_4 l & 0 \\ 0 & s_1 & 0 & s_2 l & 0 & s_3 & 0 & s_4 l \end{bmatrix} \tag{21}$$

These s_i functions can be written in terms of a non–dimensional parameter $\xi = x/l$,

$$s_1 = 1 - 3\xi^2 + 2\xi^3, \quad s_2 = \xi - 2\xi^2 + \xi^3, \quad s_3 = 3\xi^2 - 2\xi^3, \quad s_4 = \xi^3 - \xi^2 \tag{22}$$

It can be demonstrated that these shape functions contain a complete set of rigid–body modes, enabling the ANCF elements to be used in any large displacement and rotation applications such as that addressed in this paper.

4.2 Elastic forces

The neutral axis of a finite element, for any given position and deformation state defined by its vector of nodal coordinates $\mathbf{e}$, can be represented as a parametric curve $\mathbf{r} = \mathbf{r}(x)$. Since the cross–sections are assumed to remain plane and perpendicular to the neutral axis, its equation completely defines the stress and strain distributions along the finite element.

If the Green–Lagrange longitudinal strain ε_l and the curvature κ are obtained from the parametric equations of the neutral axis, the total strain energy can be calculated as,

$$U = \frac{1}{2}\int_0^l \left[EA\varepsilon_l^2 + EI\kappa^2\right] \mathrm{d}x \tag{23}$$

where A is the cross–sectional area, I is the second moment of area of the cross section, and E is the Young's modulus of the material. A cable does not have the bending stiffnes corresponding to a beam with its same cross–sectional area and, in order to simulate this behavior, a reduction factor of 25 is applied to the second moment of area I. By using the expression of the strain energy shown in Eq. (23), one can obtain the elastic forces as,

$$\mathbf{Q}_e = -\left(\frac{\partial U}{\partial \mathbf{e}}\right)^{\mathsf{T}} \tag{24}$$

Depending on the level of simplification applied to the longitudinal strain and the curvature, several longitudinal and transversal force models are derived in [1]. In the present work, the most complete models L2 and T2 described in the referred article are used, due to the large deformations that appear in the contact with the pulley.

5 CABLE–PULLEY CONTACT MODEL

5.1 Distributed contact forces

The contact forces at the cable–pulley interface are distributed along the length of the contact arc. Thus, the generalized contact forces acting on any given element are the result of integrating these distributed forces $\mathbf{f}_c$ along its length l_i,

$$\mathbf{Q}_c = \int_0^{l_i} \mathbf{f}_c(x)^T \mathbf{S}(x)\,\mathrm{d}x = \int_0^1 \mathbf{f}_c(\xi)^T \mathbf{S}(\xi) l_i\,\mathrm{d}\xi \tag{25}$$

The symbolic evaluation of this integral would require the contact forces to be expressed as a function of the material coordinate ξ. Rather than evaluating the full integral, a Gauss–Legendre quadrature is used for obtaining the generalized contact forces [11], so that the forces are only evaluated at several certain points ξ_i along the element. For an n–point quadrature, the approximated integral remains,

$$\mathbf{Q}_c \simeq \sum_{i=1}^{n} w_i \mathbf{f}_{ci}^T \mathbf{S}_i l_i \tag{26}$$

where $\mathbf{f}_{ci}^T$ and $\mathbf{S}_i$ are the contact forces per unit length and the interpolation matrices, evaluated at the corresponding Gauss–Legendre integration points ξ_i, and w_i are the Gauss–Legendre quadrature weights.

5.2 Variables defined at a contact point

Figure 4 is used to show the variables defined in order to calculate the contact forces. When a certain point of the cable, p, denoted as the *contact point*, makes its first contact with the pulley, the corresponding point of the pulley, p_{st}, whose absolute position initially coincides with that of p, is denoted as the *stiction point*. As the time integration goes on, these two points might no longer be coincident, since the stiction point moves rigidly attached to the pulley, whereas the contact point moves along with the cable. Both the stiction point and the contact point are uniquely defined by their corresponding polar angles θ_{st} and θ, as shown in the Figure. A radial position vector can be defined at each point of the neutral axis of the cable,

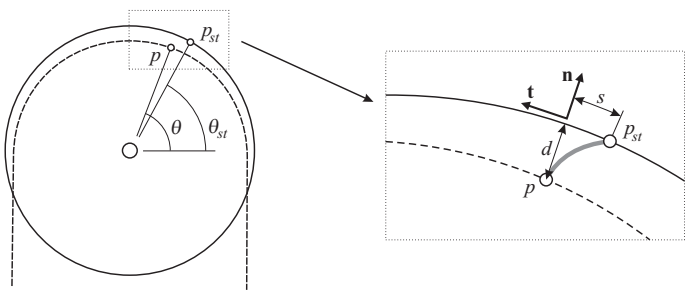

Figure 4. Normal and tangential contact model.

such that,

$$\mathbf{r}_r = \mathbf{r} - \mathbf{r}_0 \tag{27}$$

where $\mathbf{r}_0$ is the absolute position of the center of the pulley. This vector enables to define a pair of orthonormal vectors, $\mathbf{n}$ and $\mathbf{t}$, which are respectively normal and tangent to the pulley surface at the contact point, and will determine the directions of both the normal and the tangential contact forces. The radial penetration or *indentation*, d, and the tangential displacement with respect to the stiction point or *creep*, s, can be obtained as,

$$d = R - |\mathbf{r}_r|\,, \quad s = R\,(\theta - \theta_{st}) \tag{28}$$

where R is the pulley radius. Their respective time derivatives are obtained by simply projecting the absolute velocity into $\mathbf{n}$ and $\mathbf{t}$ respectively, taking into account that the pulley rotates with an angular velocity ω for calculating the creep rate $\dot{s}$,

$$\dot{d} = \dot{\mathbf{r}}^{\mathsf{T}}\mathbf{n}, \quad \dot{s} = \dot{\mathbf{r}}^{\mathsf{T}}\mathbf{t} - \omega R \tag{29}$$

5.3 Normal force model

The normal force per unit length $\mathbf{f}_n$ is introduced by means of the Hunt–Crossley contact model. The Hunt–Crossley contact model states that the normal contact force can be represented as a spring–damper pair with nonlinear damping, according to the following expression,

$$\mathbf{f}_n = k_n d^n \left(1 + D\dot{d}\right)\mathbf{n} \tag{30}$$

In this equation, k_n is the normal stiffness per unit length, and D is a damping factor. The exponent n depends on the geometry and, according to Hertz contact theory [5, 9], a value between 1 and 1.5 should be acceptable for cylinder–cylinder and cylinder–plane contacts, so that the value chosen for the cable–pulley contact is n =1. The value of D must be chosen so that $1 + D\dot{d}$ never becomes negative for the velocities appearing along the simulation since, otherwise, the normal force could pull the cable towards the pulley, which has no physical meaning.

5.4 Tangential force model

The Rooney and Deravi creep–rate–dependent friction law [5], which has been previously used for modeling belt–drives [11, 12], is no longer valid in the particular case studied in this paper, since the tangential force voids whenever no relative tangential velocity exists. Therefore, the creep–rate–dependent friction law fails to converge in the calculation of the initial static equilibrium, in the general case of the weights of the cabin and the counterweight being different.

In order to overcome this problem, the friction model implemented in the present work should be able to introduce force even when the relative tangential velocity is zero. This is achieved by modeling the frictional force $\mathbf{f}_t$ with a bristle contact model for low creep rates, whereas classic Coulomb dry friction is used for higher creep rates [3, 8]. This implies that two separate tangential force models are defined,

$$\mathbf{f}_t = \begin{cases} \mathbf{f}_{st} & \dot{s} \leq v_{st} \\ \mathbf{f}_{sl} & \dot{s} > v_{st} \end{cases} \tag{31}$$

where $\mathbf{f}_{st}$ stands for the stiction force per unit length, $\mathbf{f}_{sl}$ for the sliding force per unit length, and v_{st} is the transition relative velocity at which the switching between models occur. In order to make the model more numerically friendly, the transition between both models is made through a smooth function κ,

$$\mathbf{f}_t = \kappa\mathbf{f}_{st} + (1 - \kappa)\,\mathbf{f}_{sl} \tag{32}$$

being κ a function of $\dot{s}$ that quickly decreases from 1 to 0 around v_{st}, such as

$$\kappa = e^{-(\dot{s}/v_{st})^2} \tag{33}$$

The force in the lower velocity range is assumed to behave as a brush bristle, in such a way that the relative displacement s represents the deflection at the tip of the bristle, as depicted in Figure 4. Therefore, the tangential force can be modeled as a linear spring–damper pair in the tangential direction,

$$\mathbf{f}_{st} = -\left(k_b s + c_b \dot{s}\right)\mathbf{t} \tag{34}$$

The force is not allowed to be higher than a saturation value, determined by Coulomb's friction law,

$$f_{sat} = \mu_s f_n \tag{35}$$

where μ_s is the static friction coefficient, which is usually higher than the dynamic one. If the norm of the force obtained by using Eq. (34) exceeds the saturation value, the norm of $\mathbf{f}_{st}$ becomes f_{sat}, and the position of the stiction point is updated for making it correspond to the bristle deflection associated to the saturation force,

$$\mathbf{f}_{st} = -\operatorname{sgn}(s)\, f_{sat}\mathbf{t} \tag{36}$$

$$\theta_{st} = \theta - \operatorname{sgn}(s)\, \eta_{st} \frac{f_{sat}}{k_b R} \tag{37}$$

The function $\operatorname{sgn}(s)$ outputs 1 if s is equal or higher than zero, and -1 otherwise, and η_{st} is a factor that can improve the numerical behavior, representing the amount of bristle deflection in the saturation state. In the present work, a value of 1 is used for this parameter.

The tangential force for higher creep rates is calculated by means of a pure Coulomb's friction law, using in this case the dynamic friction coefficient μ_d,

$$\mathbf{f}_{sl} = -\operatorname{sgn}(\dot{s})\, \mu_d f_n \mathbf{t} \tag{38}$$

When the creep rate is higher than the transition velocity v_{st}, this is the dominant friction model. However, $\mathbf{f}_{st}$ is still being evaluated, so that the stiction point is correctly updated in case the stiction force reaches its saturation value.

6 NUMERICAL RESULTS

In order to compare both models, a simple elevator model consisting of a cabin and a counterweight is used. The model parameters are those shown in Table 1.

Parameter	Symbol	Value	Parameter	Symbol	Value
Pulley radius	R	0,3 m	Normal contact stiffness	k_n	$1,5 \cdot 10^7$ N/m^2
Pulley center height	H	20 m	Normal damping factor	D	10 s/m
Initial cabin height	h_i	16,5 m	Stick–slip transition velocity	v_{st}	10^{-4} m/s
Final cabin height	h_f	19,5 m	Bristle stiffness	k_b	$5 \cdot 10^6$ N/m^2
Undeformed cable length	L	5 m	Bristle viscous damping	c_b	10^3 Ns/m^2
Cable diameter	ϕ	10 mm	Dynamic friction coeff.	μ_d	0,7
Number of cables	n	5	Static friction coeff.	μ_s	0,7
Young's modulus	E	10^5 MPa	Cabin mass	m_{cab}	1000 Kg
Cable density	ρ	5095 Kg/m^3	Counterweight mass	m_{cw}	600 Kg
Motor inertia	I_m	0,5 Kg m^2			

Table 1. Parameters of the elevator model.

The ANCF model is discretized such that the contact arc is divided into 32 elements, thus making a total of 170 finite elements. The model works even with 3 elements per half pulley, but when the elements are long the transition elements, i.e. those that are entering or leaving the pulley, do not adapt well to the pulley curvature, leading to the introduction of a large–amplitude spurious vibration of the cabin, whose frequency is equal to the number of elements that enter the pulley per second. This problem is mainly due to two factors, namely the limitations of using third–order polynomials as shape functions, and the absence of shear deformations [7]. The second problem is probably the most relevant, since Kerkkanen et al., whose model includes shear deformation –at the cost of increasing the number of variables per node–, report no issues with numbers as low as 4 elements per half pulley. Therefore, the elimination of the shear deformation does not actually improve the efficiency since the number of finite elements must be increased by a large amount.

The maneuver starts at an equilibrium position with the cabin placed at $h_i = 16,5$ m. In order to lift the cabin up to a final height of 19,5 m, the following law is used for the guidance of the pulley:

$$\ddot{\omega} = \begin{cases} 1/R & 0 \leq t < 1 \\ -1/R & 1 \leq t < 2 \\ 0 & 2 \leq t < 3 \\ -1/R & 3 \leq t < 4 \\ 1/R & 4 \leq t \leq 5 \end{cases} \tag{39}$$

where the angular jerk $\ddot{\omega}$ is expressed in rad/s^3 and time t is expressed in seconds.

Figure 5 shows in the two upper plots the vertical vibrations of the cabin, which correspond to y_{cab} and $\dot{y}_{cab}$ in the semi–analytical model. It is observed that the elongation decreases with the cable length in the semi–analytical model, as expected since the stiffness is inversely proportional to the cable length. In the ANCF model the elongation is roughly constant because there exists a small amount of slip that compensates for this effect. Actually, the elongation calculated in the ANCF model is no longer an elongation but a difference between where the cabin is and where it would be in case of an non–deformable cable without slip. In the velocity graph, it is observed that the amplitude of oscillation is much smaller in the ANCF model; this happens due to the fact that the semi–analytical model has no damping, whereas the ANCF model introduces damping in the contact and, moreover, it needs a small amount of numerical dissipation added via a Newmark integrator [2].

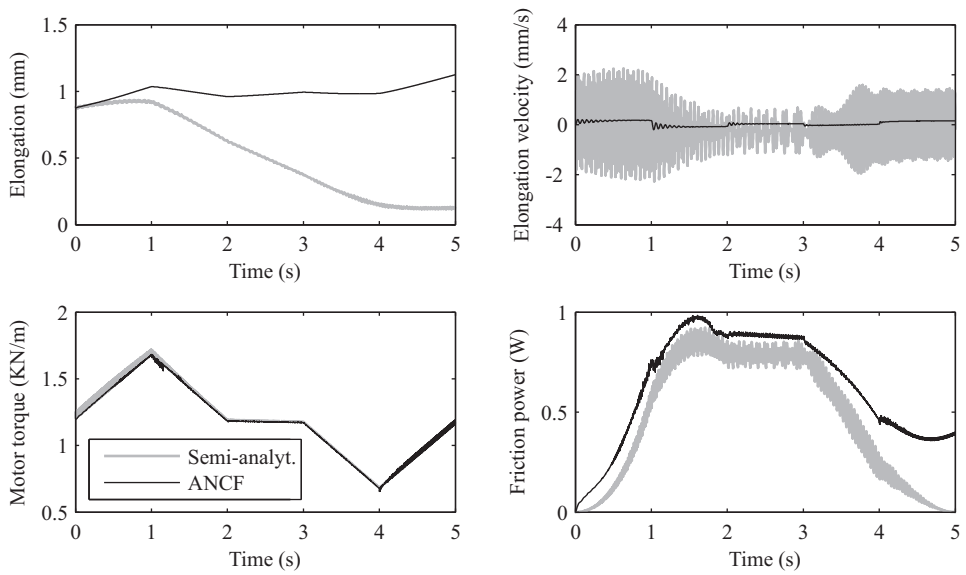

Figure 5. Simulation results.

In the lower graphs of Figure 5 the motor torque and the instantaneous power dissipated by the friction forces are plotted. In the case of the motor torque the agreement between both plots is very good. The dissipated power shows a reasonable agreement, but it is sensitive to the contact parameters so that the results are not conclusive. Anyway, the maximum power lies always anywhere between 0,5 and 1,5 kW, so the order of magnitude of the friction forces is not very different. It is observed that the friction power is not equal to zero at the end of the simulation in the ANCF model. This happens because when the pulley stops, the cable keeps sliding with a decreasing velocity, so that it is not completely static at $t = 5s$. In what respects the distribution of contact forces, the results are very similar to those obtained by Kerkkanen et al.

7 CONCLUSIONS

The semi–analytical model shows a very good behavior, being a very fast and accurate method for simulating weight lifting machines. The main drawbacks of this model are that it is an ad–hoc model for a specific

configuration, and it does not account for a possible cable slip. On the other hand, the ANCF model is a very general and robust method for modeling the cable–pulley interaction, although it cannot correctly model the curvature of the transition elements, leading to higher numbers of finite elements that ultimately mean less performance than with shear–deformation–capable elements as done by Kerkkanen et al. Moreover, internal damping should be added to the cable [6], in order to avoid the artificial introduction of numerical damping into the integrator.

ACKNOWLEDGEMENTS

The second author thanks the support of the Spanish Ministry of Education and Science under project reference TRA2007-66808.

REFERENCES

[1] BERZERI, M., AND SHABANA, A. A. Development of simple models for the elastic forces in the absolute nodal co–ordinate formulation. *Journal of Sound and Vibration 235*, 4 (2000), 539–565.

[2] CUADRADO, J., DOPICO, D., NAYA, M. A., AND GONZÁLEZ, M. Penalty, semi–recursive and hybrid methods for MBS real–time dynamics in the context of structural integrators. *Multibody System Dynamics 12*, 2 (2004), 117–132.

[3] DOPICO, D., LUACES, A., GONZÁLEZ, M., AND CUADRADO, J. Dealing witn multiple contacts in a human–in–the–loop application. In *ECCOMAS Thematic Conference: Multibody Dynamics 2009* (Warsaw, Poland, 2009).

[4] ESCALONA, J. L., HUSSIEN, H. A., AND SHABANA, A. A. Application of the absolute nodal coordinate formulation to multibody system dynamics. *Journal of Sound and Vibration 214*, 5 (1998), 833–851.

[5] FLORES, P., AMBRÓSIO, J., CLARO, J. C., AND LANKARANI, H. *Kinematics and Dynamics of Multibody Systems with Imperfect Joints*. Springer–Verlag, Berlin, 2008, ch. 3, pp. 47–66.

[6] GARCÍA-VALLEJO, D., VALVERDE, J., AND DOMÍNGUEZ, J. An internal damping model for the absolute nodal coordinate formulation. *Nonlinear Dynamics 42*, 4 (Dec. 2005), 347–369.

[7] GERBERT, G. Belt slip – a unified approach. *Journal of Mechanical Design 118*, 3 (1996), 432–438.

[8] GONTHIER, Y., MCPHEE, J., LANGE, C., AND PIEDBŒUF, J.-C. A regularized contact model with asymmetric damping and dwell–time dependent friction. *Multibody System Dynamics 11*, 3 (2004), 209–233.

[9] HUNT, K. H., AND CROSSLEY, F. R. E. Coefficient of restitution interpreted as damping in vibroimpact. *Journal of Applied Mechanics 7* (1975), 440–445.

[10] JOHNSON, K. L. *Contact Mechanics*. Cambridge University Press, Cambridge, UK, 1987.

[11] KERKKÄNEN, K., GARCÍA-VALLEJO, D., AND MIKKOLA, A. Modeling of belt–drives using a large deformation finite element formulation. *Nonlinear Dynamics 43*, 3 (2006), 239–256.

[12] LEAMY, M. J., AND WASFY, T. M. Analysis of belt–drive mechanics using a creep–rate–dependent friction law. *Journal of Applied Mechanics 69*, 6 (2002), 763–771.

[13] SHABANA, A. A. *Dynamics of Multibody Systems*. Cambridge University Press, New York, NY, USA, 1998.

[14] ČEPON, G., AND BOLTEŽAR, M. Dynamics of a belt–drive system using a linear complementarity problem for the belt–pulley contact description. *Journal of Sound and Vibration 319*, 3–5 (2009), 1019–1035.